PACS Spectroscopy performance and calibration

PICC-KL-TN-041

Prepared by	Bart Vandenbussche	
With inputs by	Alessandra Contursi Helmut Feuchtgruber Katrina Exter Christophe Jean Albrecht Poglitsch Elena Puga Pierre Royer Roland Vavrek	
Approved by		
Authorised by		

Distribution List

Recipients	*Affiliation*	*Nr. of Copies*

Document Change Record

Issue	*Date*	*Description*
1.0	10. Mar. 2010	First version limited to flux calibration accuracies and gross correction factors to the ground flux calibration
1.1	11. Mar. 2010	Incorporated comments + added a few clarifications
2.0	6. Apr. 2011	Updated flux calibration error budget; included beam efficiencies
2.1	25. May. 2011	Included 2nd pass ghosts; formatting for public release
2.2	26. May. 2011	Included unchopped spectroscopy uncertainties, beam size as a function of wavelength
2.3	31. May. 2011	Included Wavelength calibration section
2.4	16, June 2011	Included chopped and unchopped comparison examples.
3.0	7. July 2016	Update for SPG 14.2

Table of Contents

1 Introduction

This document provides details on the calibration accuracy and the necessary information to optimally interpret PACS spectroscopy observations.

The present version (3.0) of this document is applicable for PACS results obtained with the legacy standard product generation pipeline and hipe software release versions 14.2 and PACS calibration files version 77.

Processing software version can be verified in the FITS header (CREATOR keyword) or in hipe under help -> about hipe

The version of the set of calibration files used for the processing can be found in the FITS header (calTreeVersion keyword) or in hipe with the command `print (getCalTree())`

2 Flux calibration

2.1 Two flux calibration schemes: Calblock and Telescope background

The PACS flux calibration uses two schemes: chopped measurements use the 'off' chopping positions, which are measurements of the telescope emissivity, throughout the observation to derive the instantaneous detector response at any given time during the observation. The measured signal of the telescope background is compared to the expected emissivity from an empirical model of the telescope emissivity that was fitted to full range spectra of Ceres and Pallas throughout the mission. The absolute scale of the emissivity model was corrected to the 109 PACS key-wavelength flux calibration measurements of fiducial stars and asteroids.

For unchopped measurements, the detector response is determined from the calibration block, a measurement on the internal calibration source at the start of the observation. The emissivity of the internal calibration source was calibrated against the 109 PACS key-wavelength flux calibration measurements of fiducial stars and asteroids.

2.2 Flux calibration accuracies

The PACS spectrometer flux calibration accuracy is limited by detector response drifts and slight pointing offsets. These limit both the absolute flux accuracy and relative accuracy within a band.

2.2.1 Absolute flux calibration accuracy

This accuracy applies for single line fluxes or continuum flux densities at a given wavelength in any spaxel. Beware of the correction needed for flux falling out of the pixel for point sources (section Error: Reference source not found).

The absolute flux calibration accuracy was assessed by comparing the measured flux density at key wavelengths in every band to the expected (model) flux density for over 100 measurements of fiducial calibration stars and asteroids. This is depicted in Figures 1 and Figure 2 for two PACS spectral bands.

- The standard deviation of the ratio measured/expected flux density over all measurements is 6 to 12% in all bands.
- The systematic error is 1%.

One fiducial calibration star, HD161796, was measured 120 times in chopped mode, 5 times in unchopped mode. These observations allow to assess the continuum flux reproducibility as depicted in Figures 3 and 4 for two spectral bands.

- The stochastic error (standard deviation) on the reproducibility is better than 4%
- The peak to peak reproducibility variations are better than 15%.

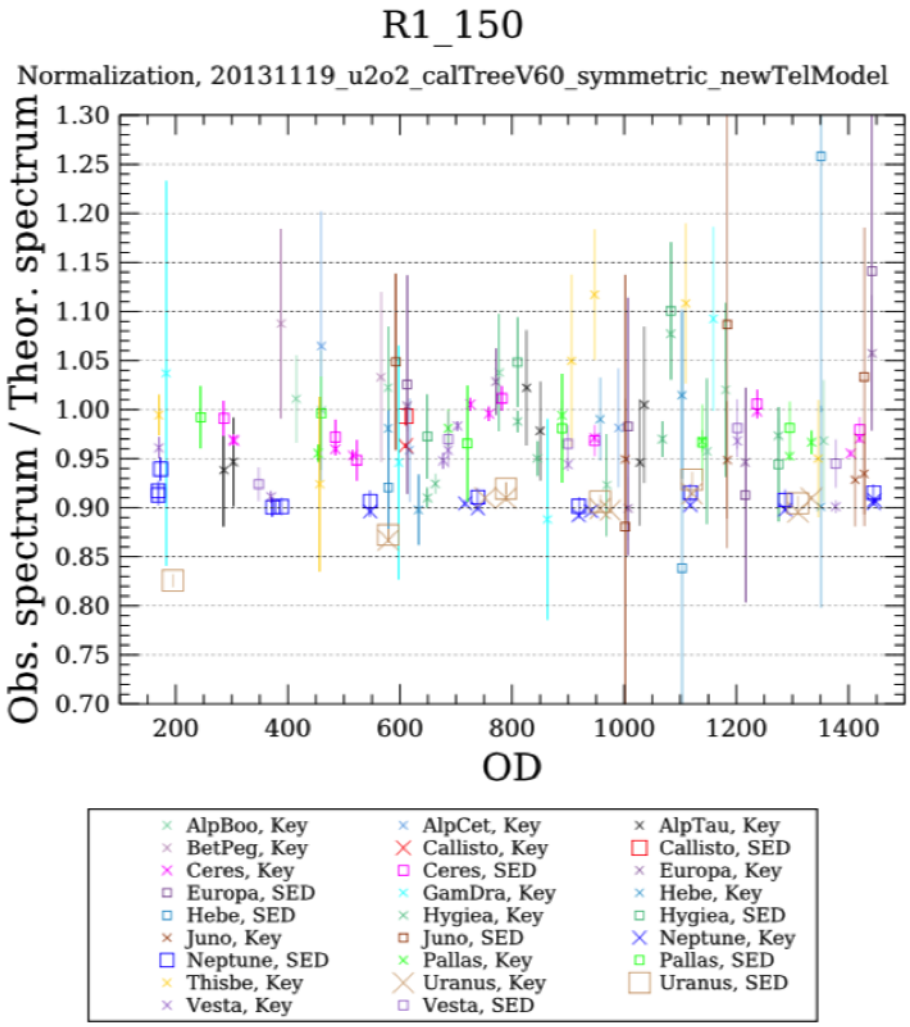

Figure 1: Comparison of observed versus expected flux of all key wavelength observations of celestial flux calibrators in band R1.

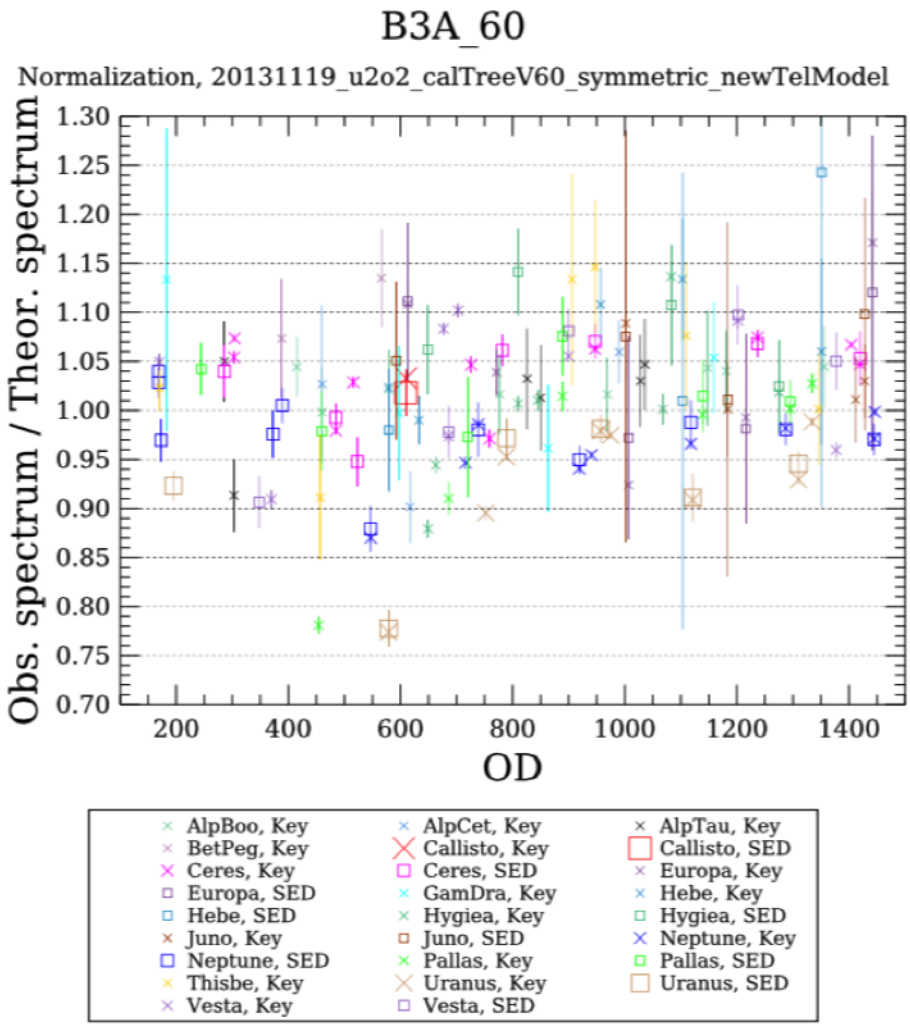

Figure 2: Comparison of observed versus expected flux of all key wavelength observations of celestial flux calibrators in band B3A

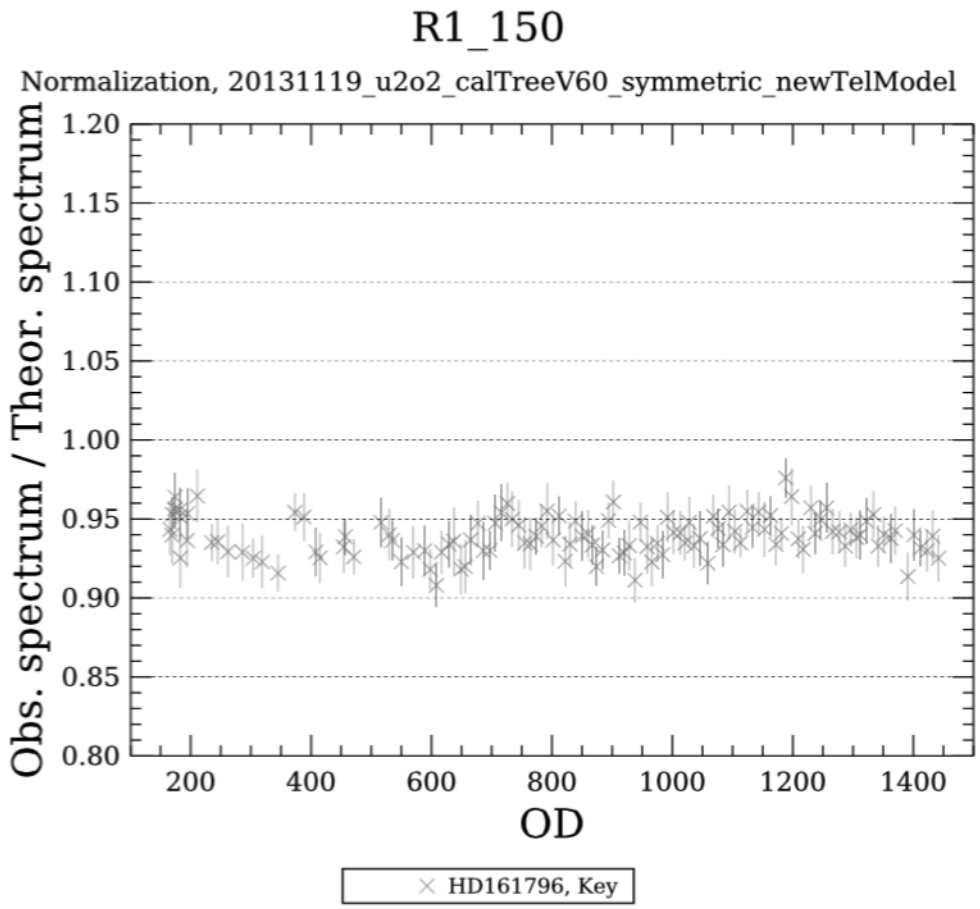

Figure 3: Reproducibility measurements of HD161796 in band R1

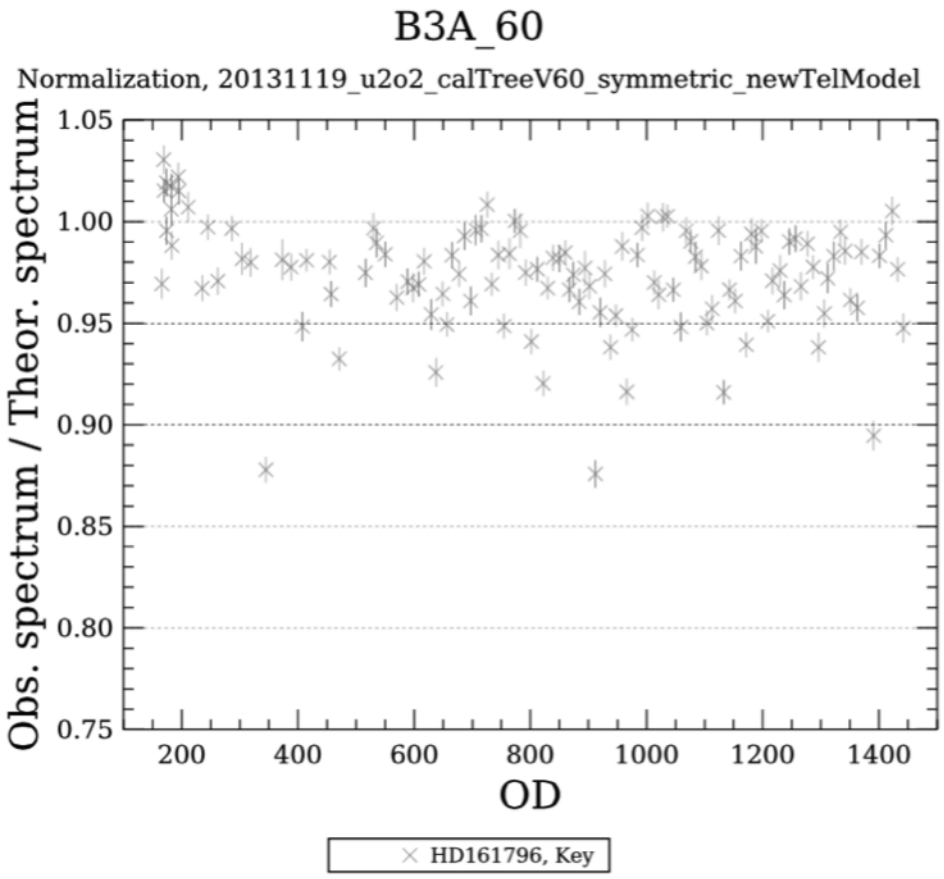

Figure 4: Reproducibility measurements of HD161796 in band B3A

2.2.2 Relative flux accuracy within a band and detection limit for broad features

Broad spectral features (a few micrometer) and continuum shape difference can be introduced by transient effects and pointing offsets. Note that due to the origin of these effect, they will be seen differently in every observation, so dividing two PACS spectra will not eliminate these instrumental effects.

For **chopped** observations, where the telescope background normalisation calibration scheme is used, the relative flux accuracy within a band is:

- 5% shortward of 150um
- 10% longward of 150um.

For unchopped observations, where the calibration block calibration scheme is used, the relative flux accuracy within a band is:

- 10% across the PACS wavelengh range

This is the relative accuracy to assume when comparing relative line fluxes within a spectral band. When comparing line fluxes across spectral bands, the absolute flux accuracies in section 2.2.1 apply.

The relative in-band accuracy is also the limit on detection of broad spectral features (solid state features, dust continuum shape).

These numbers apply to the wavelength regions not affected by spectral leakage (see section 4)

Applying the interactive pointing correction in hipe can potentially improve the relative in-band accuracy.

The in-band accuracies were determined from repeated measurements of the asteroid Pallas in the course of the Herschel mission. The observation/model residuals (normalised to the flux at the key wavelength of the band) of the different observations are depicted in Figure 5.

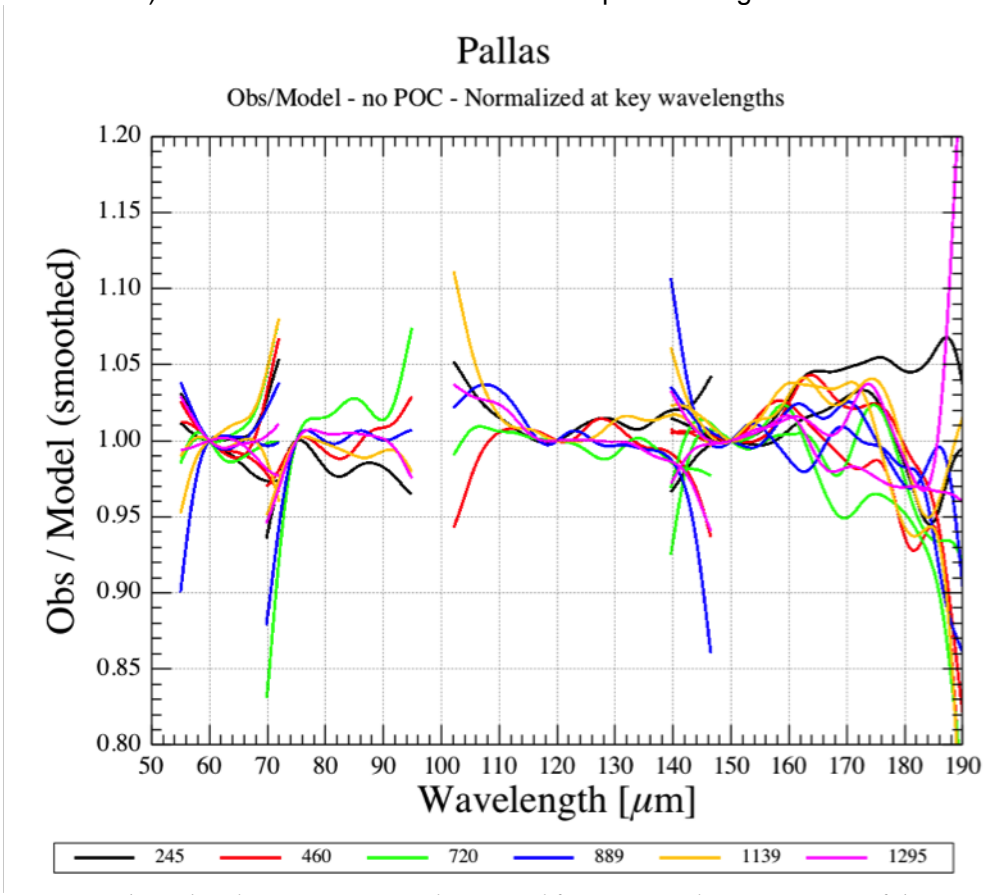

Figure 5: The in-band accuracies were determined from repeated measurements of the asteroid Pallas in the course of the Herschel mission. The observation/model residuals (normalised to the flux at the key wavelength of the band) of the different observations are shown in different colors; numbers in the legend are the OD of the respective observations.

3 PACS spectrometer beam efficiency

3.1 Detector sampling of the PSF

The PACS spectrometer spaxels sample a part of the PSF delivered by the Herschel telescope. The telescope PSF becomes larger with wavelength, and shows substantial departure from a gaussian profile due to the telescope wavefront errors, mainly caused by the three-point mount of the telescope dish. At different wavelengths, different fractions of the PSF structure are seen by the different spaxels. This is illustrated in Figure 6.

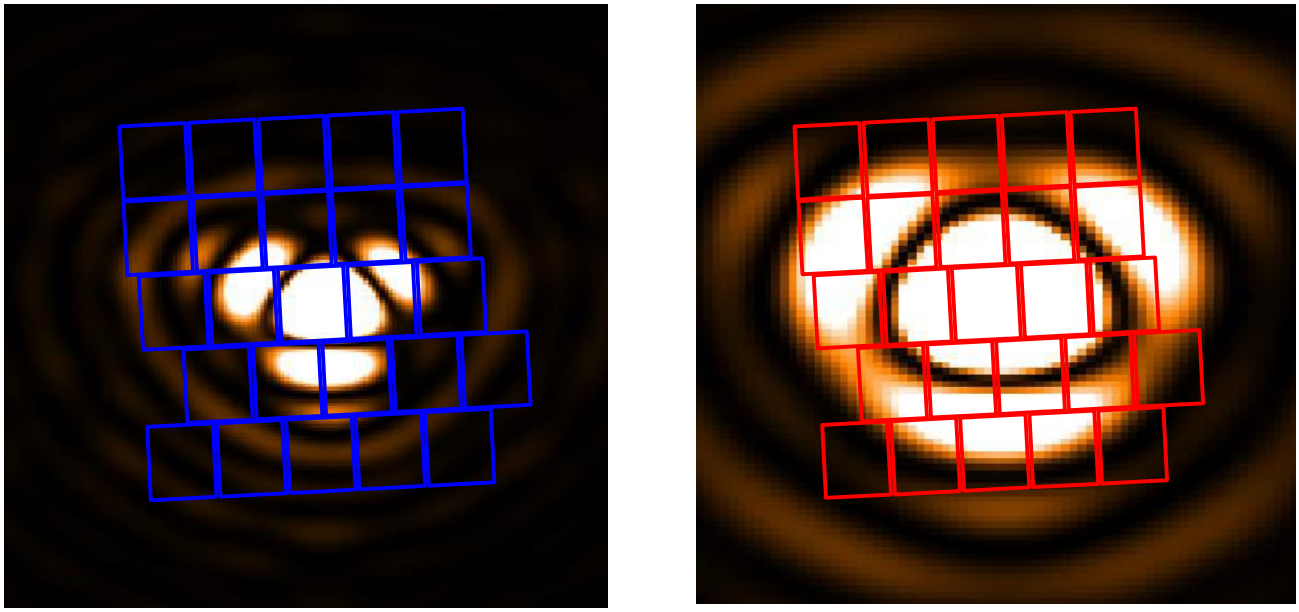

Figure 6: Figure 1: PACS spectrometer detector positions overlaid on the telescope PSF at 75um (left) and 150um (right). Color scaling of the PSF is chosen to enhance the lobes and wings of the psf.

Given the pointing accuracy of the spacecraft, this means that the fraction of the PSF falling onto the central spaxel can vary substantially. This is presently the main limitation of the flux calibration.

3.2 Measured beam efficiencies

The beam efficiencies have been measured via raster maps on Neptune at a few selected wavelengths.

The measured beam maps measured in every spaxel have been made available on the HSC PACS web page and are also included as calibration products in the PACS calibration product tree.

In figure 7 we show the measured beam efficiencies at 62, 75, 125 and 150um. Figure 8 shows the gaussian width of the measured beams as a function of wavelength.. The pixel size dominates the width of the beam efficiency up to 150um.

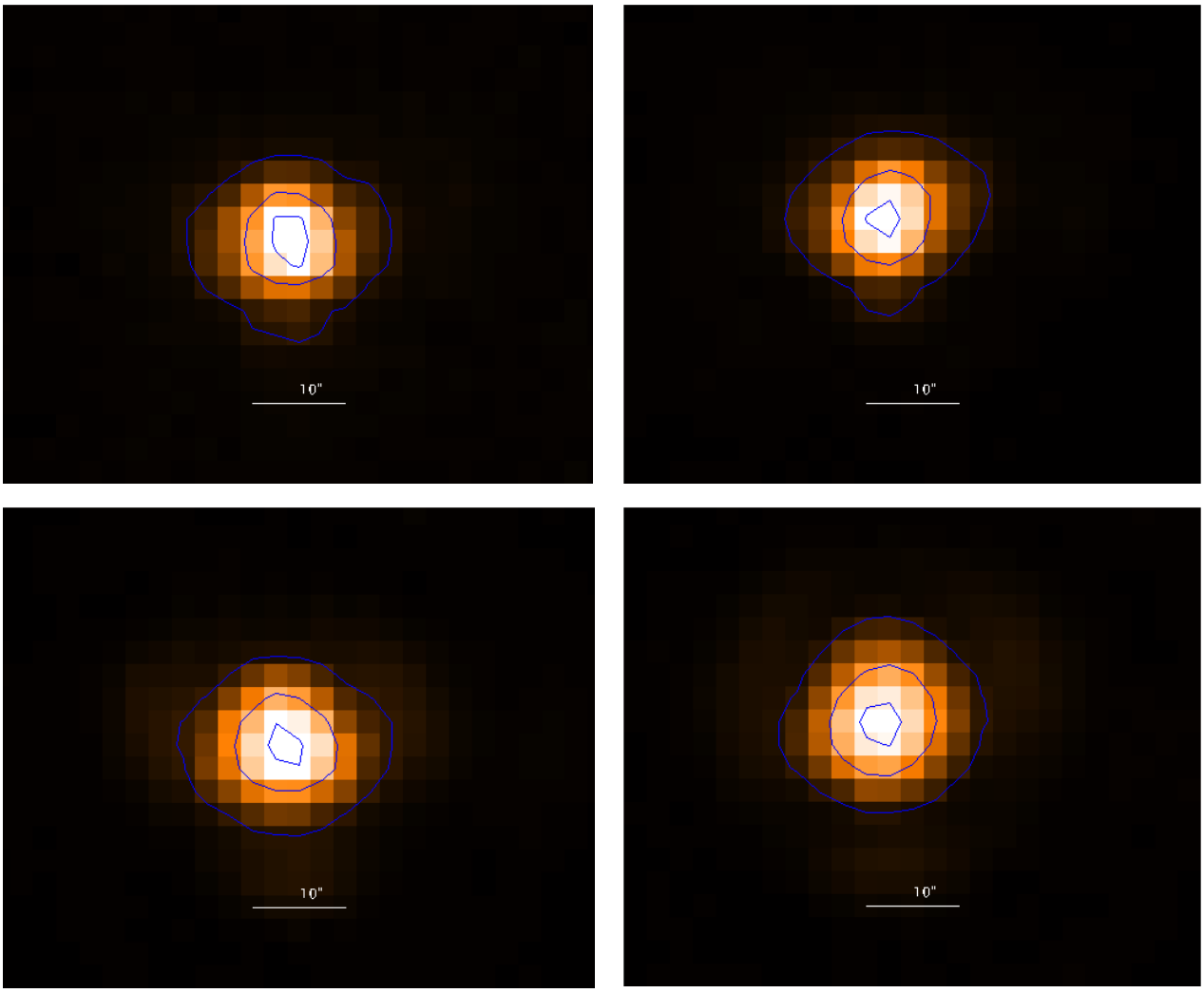

Figure 7: PACS spectrometer beam efficiency as measured from oversampled raster maps on Neptune. From top left, to bottom right: 62um, 75um, 125um, 150um. The contours indicate 10%, 50% and 90% of the peak response.

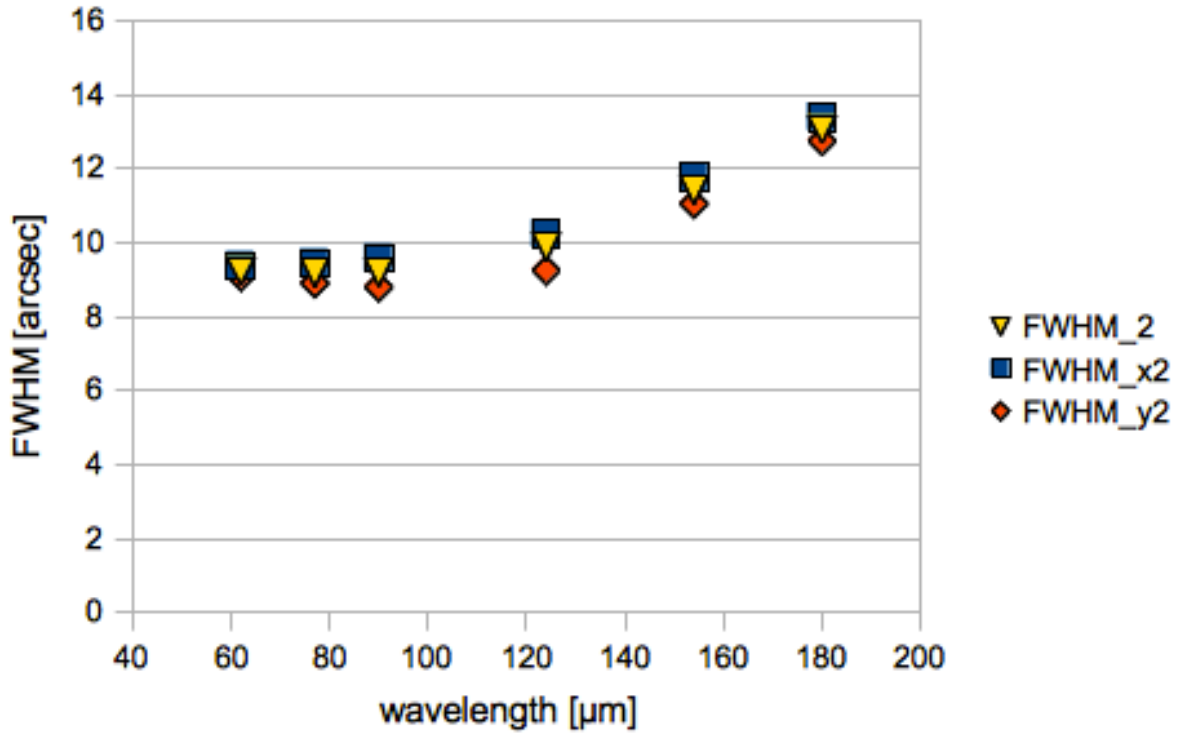

Figure 8: Width of the PACS spectrometer beams as a function of wavelength. We show the FWHM in two directions of the assymetric 2D gaussian fit (blue squares, red diamonds) and the mean of the two (yellow triangles). Note that the beams are not gaussian, these numbers are a rough indication of the beam size only,.

4 Spectral leakage and ghosts

4.1 First-pass spectral leakage seen in all spaxels

The order selection filters of the PACS spectrometer have a steep but not perfectly vertical transmission profile a the cut-off wavelengths of the spectral bands. The PACS spectra near the band borders of Bands R1, B3A and B2B are affected by higher or lower order wavelengths leaking into the spectra. Interpretation of spectral features (unresolved or continuum fluxes) in the spectral leakage regions should be avoided without consulting a PACS expert. Figures 9 - 11 show the wavelength regions affected. Band B2A is not affected by spectral leakage.

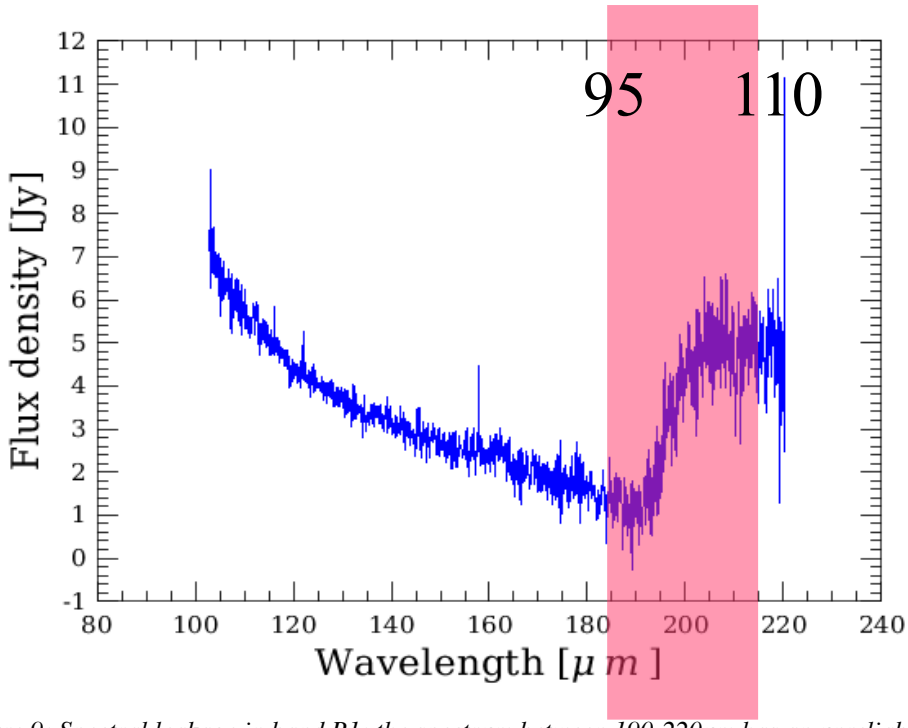

Figure 9: Spectral leakage in band R1: the spectrum between 190-220um has an unreliable (line) flux calibration, and shows superimposed spectral features from order 2 (95-110um).

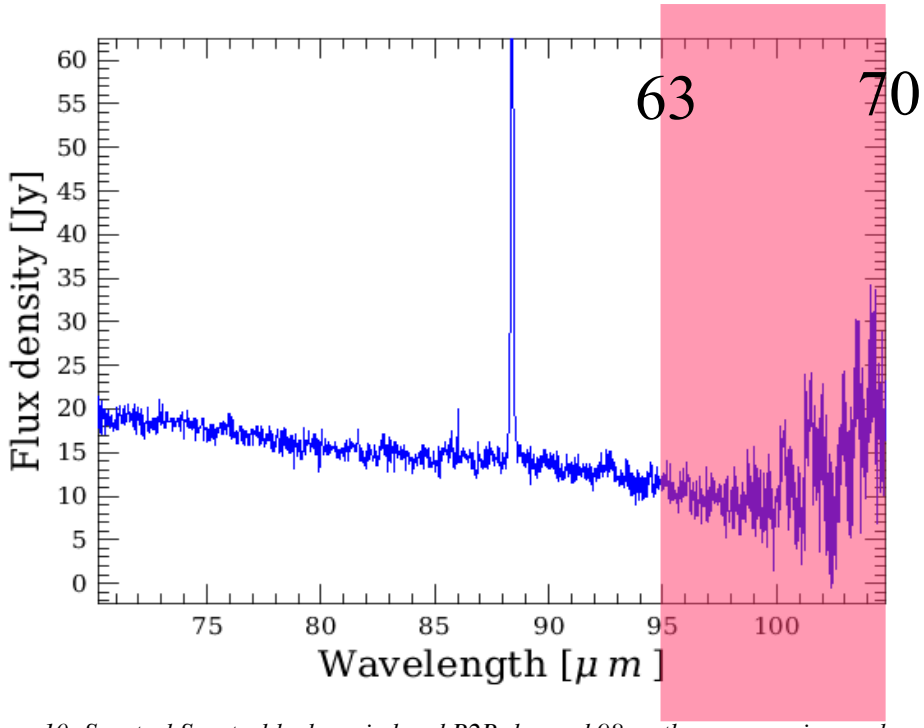

Figure 10: Spectral Spectral leakage in band B2B: beyond 98um the response is very low, and spectral features from order 3 (63-70um) are superimposed on the spectrum

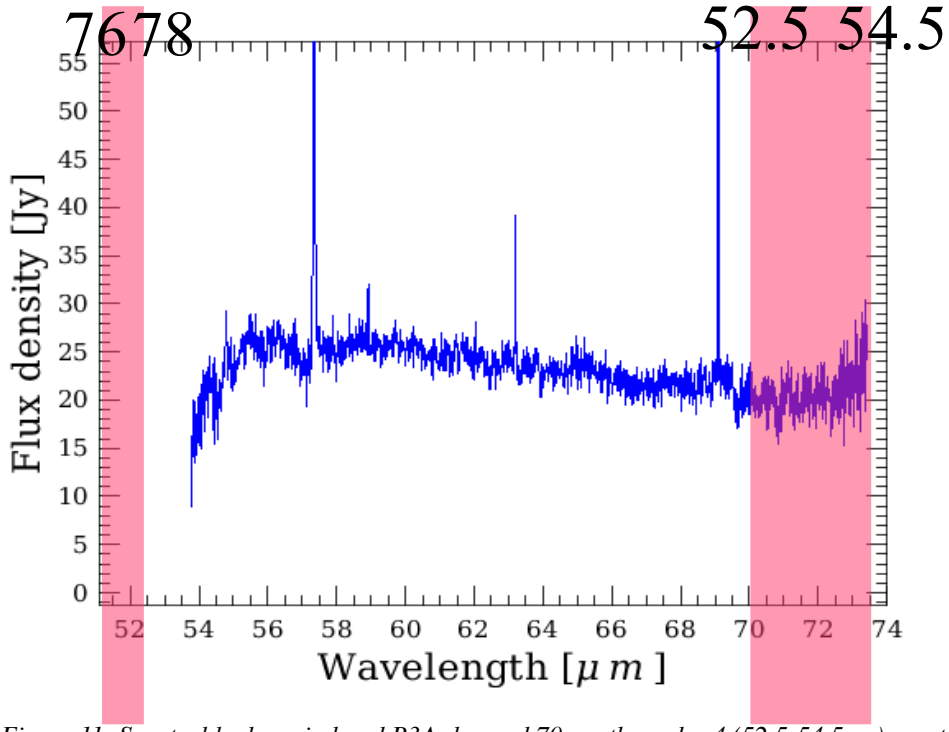

Figure 11: Spectral leakage in band B3A: beyond 70um, the order 4 (52,5-54.5um) spectrum is added to the 70-73um order 3 spectrum. This leakage can be seen down to 69um in case of an extremely bright line at 52 um , as in the spectrum shown here. The 51-52 order 3 spectrum also shows the 76-78um order 2 spectrum.

4.2 Second-pass ghost seen in some non-central spaxels

A second pass in the optics of the PACS spectrometer can cause a ghost image on some spaxels. Figure 12 shows the spaxels where a second pass ghost might appear, and the location of the corresponding spaxels where the originating, real emission is located. The ghost appears shifted in wavelength.

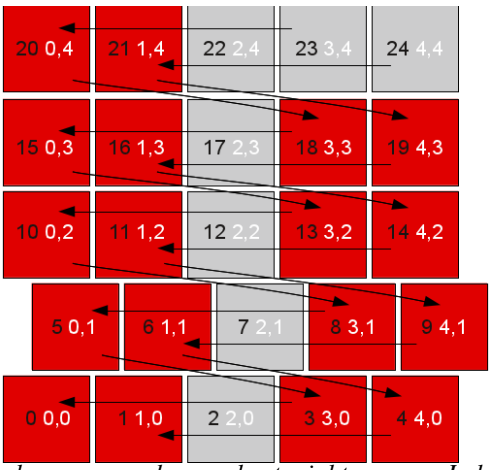

Figure 12: Location of the spaxels where a second pass ghost might appear. In black are the module numbers (this is the numbering in the PACS frames product), in white the row and column numbers in the PACS cube products. The arrows indicate the spaxel where the originating, real emission is located.

If a source in one of the originating spaxels shows a strong spectral line, typically an atomic fine structure line, a weak, broadened line can be seen at an offset wavelength in the corresponding spaxel affected by 2nd pass ghosts. The peak flux of this line is typically ~5% of the line peak of the originating line. The integrated line flux can be up to ~14% of the integrated line flux of the originating line. An example is shown in figure 15. The wavelength offset between the originating line and the ghost line depends on the spectral order of the band, and varies with wavelength. A few examples for the strongest fine structure lines in the PACS wavelength range are given in table 1. Appendix A tabulates ghost wavelength against originating wavelength for all PACS bands affected.

Before interpreting broad spectral lines in spaxels potentially affected by the 2 nd pass ghosts, observers should use these tables and, if available, the spectra observed in the corresponding ghost source spaxel, for the presence of a strong line at the originating wavelength.

Point source observations, well centered on the central spaxel, are not affected. The central column of the IFU is not contaminated by 2nd pass ghosts.

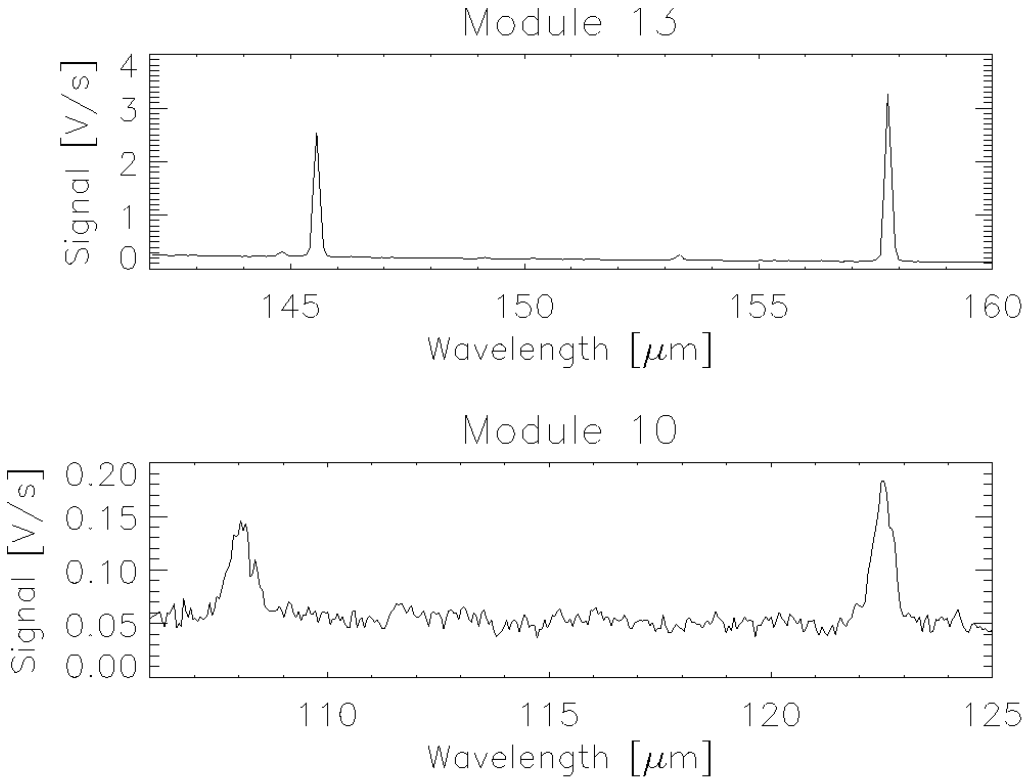

Figure 13: Example of the second pass spectral leak: the strong (real) line emission at 145.5 (OI) and 157.7 (CII) in module 13 leak into module 10, where they are seen as broadened spectral lines around 108 and 122 micron.

Band	Originating line	wavelength	ghost wavelength
B3A	O I	63.2	54
B2B	O III	88.4	72
R1	O I	145.5	108
R1	CII	157.7	122
R1	N II	205.3	178

Table 1: Example 2nd pass ghost wavelengths corresponding to prominent fine structure lines in the PACS wavelength range

5 Wavelength calibration

5.1 Wavelenght calibration accuracy

The PACS wavelength calibration relates the diffraction grating position to the wavelength seen in every detector pixel. This calibration was derived from laboratory measurements of a water vapour absorption cell, and further refined in-flight based on fine structure lines in planetary nebulae. For ideal extended sources the required accuracy of better than 20% of a spectral resolution element is met throughout all bands. While at band borders, due to leakage effects and lower S / N, the RMS calibration accuracy is closer to 20%, values even better than 10% are obtained in band centres.

For point sources the wavelength calibration may be dominated by pointing accuracy.

5.2 Wavelength shifts with source position

The 5x5 PACS spaxels of the integral field unit are imaged onto a 1D-slit. The 1D-slit image is then dispersed by the diffraction grating. As with any diffraction grating spectrometer, moving the source center with respect to the slit center in the dispersion direction will result in a slight shift of the wavelength seen in a detector pixel. Therefore, lines observed in a point source with PACS will appear slightly shifted in wavelengths if the source is not perfectly centered on the spaxel. This is illustrated in figure 14. Since the PSF peak is resolved in the slit, a distinct skew can be seen as well when the source is near or beyond the spaxel edge. These features should be taken into account before interpreting wavelength shifts or line profiles in terms of velocity. Pointing offsets along the dispersion direction do not result in a wavelength shift. The sign (red or blu-shift) and magnitude of the shift for different wavelenths is shown in figures 15and 16.

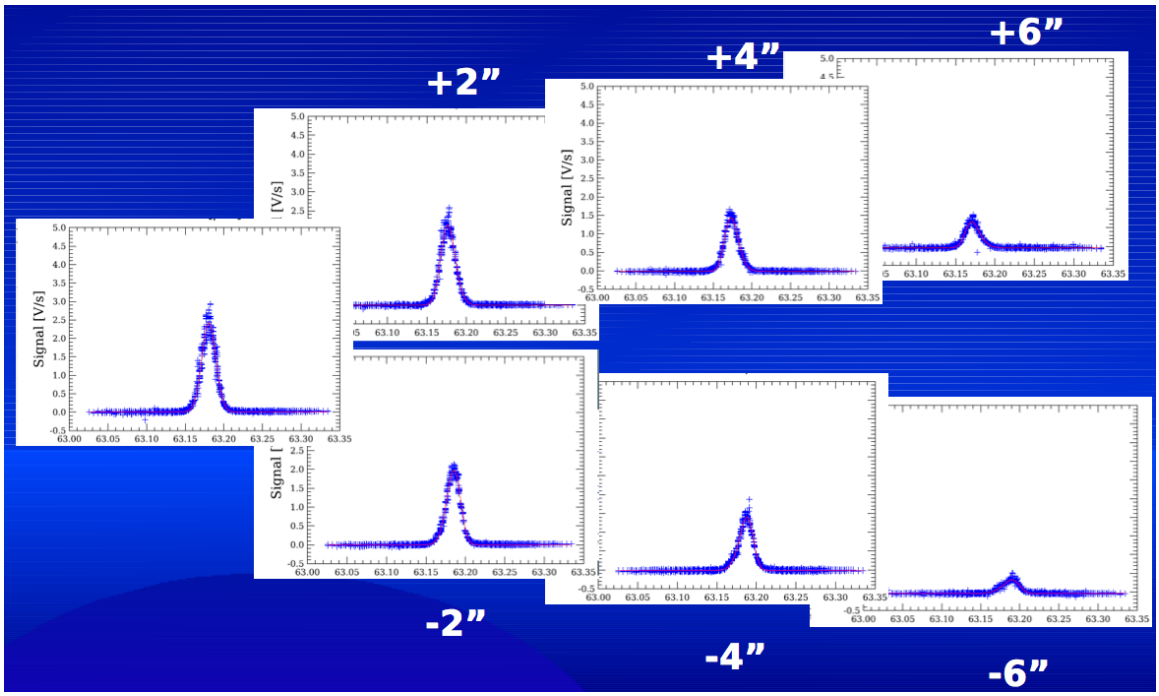

Figure 14: When a point source is offset in dispersion direction with respect to the center of a spaxel, the observed lines will show a distinct shift in wavelength and a skew.

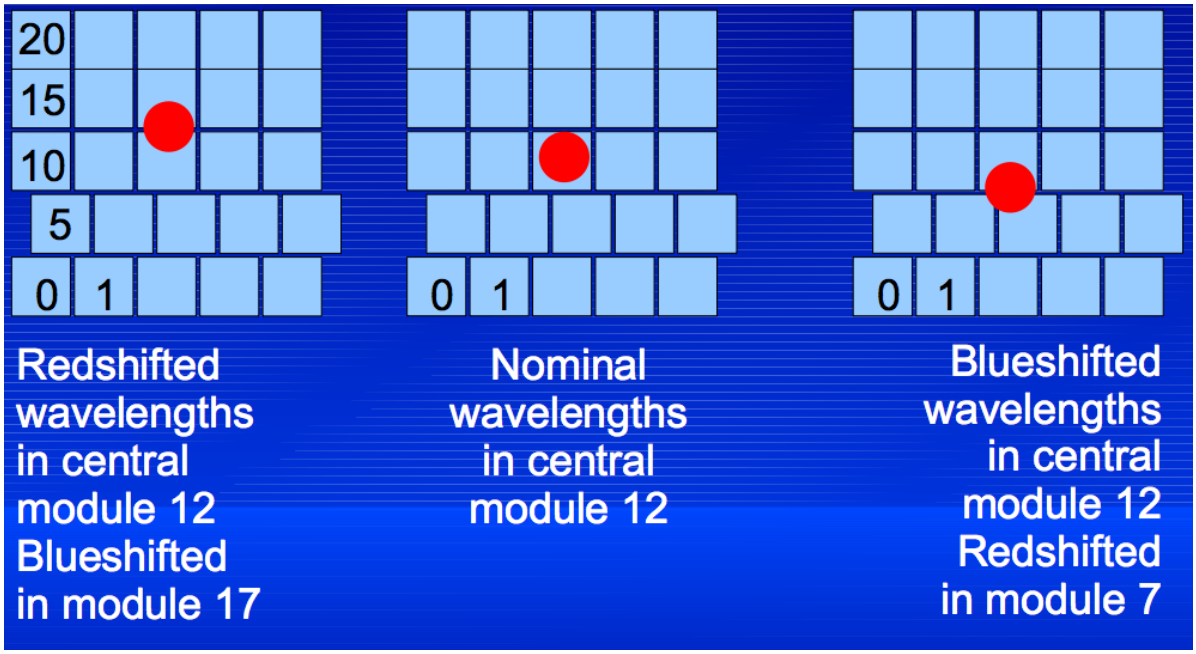

Figure 15: If a point source is offset in dispersion direction, wavelengths will be shifted to the red when moving 'up', e.g. from module 12 to module 17 in the PACS IFU. When the source is offset 'down', the wavelengths will be blueshifted.

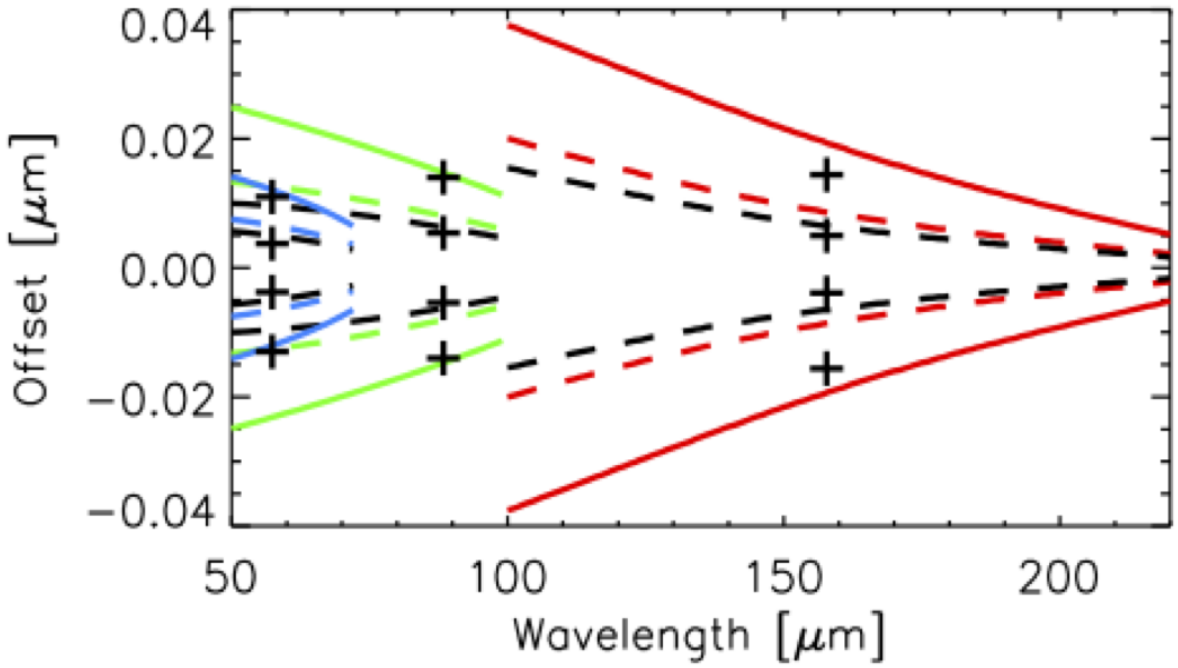

Figure 16: The wavelength shift, seen when a point source is not centered perfectly, depends on the observed wavelength and band, and the pointing offset. The black dashed line shows the wavelength shift seen for a point source offset by 1.5". The blue, green and red dashed line shows the wavelength shift for a pointing offset of 2". The solid red, green and blue line show the wavelength shift seen when the source is centered on the spaxel edge.

A.Second-pass ghosts - wavelength offsets

In the table below we list for each band the correspondence between wavelength at which a second pass ghost is seen, and the wavelength of the originating emission. See section 4.2.

Band R1	
ghost wavelength	originating wavelength
102	140.2
103	141.1
104	141.9
105	142.8
106	143.6
107	144.5
108	145.4
109	146.2
110	147.1
111	147.9
112	148.8
113	149.6
114	150.5
115	151.3
116	152.2
117	153.0
118	153.9
119	154.8
120	155.6
121	156.5
122	157.3
123	158.2
124	159.0
125	159.9
126	160.7
127	161.6
128	162.4
129	163.3
130	164.1
131	165.0
132	165.9
133	166.7
134	167.6
135	168.4
136	169.3
137	170.1
138	171.0
139	171.8
140	172.7
141	173.5
142	174.4
143	175.3
144	176.1
145	177.0
146	177.8
147	178.7
148	179.5
149	180.4
150	181.2
151	182.1
152	182.9
153	183.8
154	184.7
155	185.5
156	186.4
157	187.2
158	188.1
159	188.9
160	189.8
161	190.6
162	191.5
163	192.3
164	193.2
165	194.0
166	194.9
167	195.8
168	196.6
169	197.5
170	198.3
171	199.2
172	200.0
173	200.9
174	201.7
175	202.6
176	203.4
177	204.3
178	205.2
179	206.0
180	206.9

Band 2B	
ghost wavelength	originating wavelength
68	84.6
69	85.5
70	86.3
71	87.2
72	88.0
73	88.9
74	89.7
75	90.6
76	91.4
77	92.3
78	93.1
79	94.0
80	94.8
81	95.7
82	96.5
83	97.4
84	98.2
85	99.1
86	99.9
87	100.8
88	101.7
89	102.5

Band B3A	
ghost wavelength	originating wavelength
50	59.9
51	60.7
52	61.5
53	62.4
54	63.2
55	64.0
56	64.8
57	65.6
58	66.4
59	67.2
60	68.1
61	68.9
62	69.7
63	70.5
64	71.3
65	72.1
66	73.0
67	73.8